Proc. Natl. Acad. Sci. USA
Vol. 82, pp. 2148–2152, April 1985
Medical Sciences

In vivo solvent-suppressed localized hydrogen nuclear magnetic resonance spectroscopy: A window to metabolism?

(lactate/surface coil/chemical imaging/brain/chemical shift)

PAUL A. BOTTOMLEY, WILLIAM A. EDELSTEIN, THOMAS H. FOSTER, AND WILLIAM A. ADAMS

General Electric Corporate Research and Development Center, P.O. Box 8, Schenectady, NY 12301

Communicated by Charles P. Bean, November 26, 1984

ABSTRACT **Solvent-suppression NMR techniques are combined with a pulsed magnetic field gradient and surface coil detection method of spatial localization. The result is a technique that enables observation of metabolites in the hydrogen (^{1}H) NMR chemical-shift spectra from preselected disk-shaped volumes of biological tissue *in vivo*. Localized spectra are recorded from the normal human brain and forearm and from a dog in acquisition periods of 2 s using a 1.5-T imaging/spectroscopy system. This is several hundredfold faster than acquiring similar state-of-the-art ^{31}P NMR spectra of brain metabolites *in vivo*. Spectroscopy experiments are followed by conventional surface coil imaging sequences to precisely define the selected volume. Contamination of spectra by lipid resonances is a problem.**

Localized phosphorus (^{31}P) NMR is proving a valuable tool in the *in vivo* investigation of animal models of stroke (1–5), myocardial ischemia (6–8), tumors (9, 10), and the efficacy of drug therapy (11, 12) as well as human muscular metabolic diseases (13–15) and cerebral disorders in neonates (16). Its value resides in the ability to detect and monitor intracellular pH and *in vivo* concentrations of metabolites such as phosphocreatine (*P*Cr), ATP, and P_i, which directly measure the state of health of tissue. A major impediment limiting utility of this technology in clinical medicine is the low sensitivity of the ^{31}P resonance. Thus, data acquisition times are typically of the order 10 min for a single coarsely resolved localized volume of the order 20 cm^3 in the currently available large-aperture, 1.5- to 2-T, magnet-based spectroscopy systems (16–18).

Nucleus for nucleus, the hydrogen (^{1}H) resonance offers a 15-fold improvement in signal-to-noise ratio (19, 20) or a reduction by a factor of 227 in signal averaging time over ^{31}P NMR at the same magnetic field strength. ^{1}H NMR spectra can reveal the relative concentrations of the total *P*Cr/creatine (Cr) pool, phosphocholine (*P*Cho), *N*-acetylaspartate (*N*-AcAsp), some lipid (—CH_2—), and lactate metabolites. Such resonances have been detected *in vivo* in rat brain (21) and isolated perfused heart spectra at 8.5 T (22) and recently in rabbit brain at 1.9 T (23), all with spectral averaging times of 2–2.5 min and sample volumes of the order 1–10 cm^3. The amplitude of the lactate (—CH_3) resonance appears as sensitive to hypoxia and ischemia as the P_i resonance in ^{31}P spectra and contains 3-fold as many nuclei. Thus, localized *in vivo* ^{1}H NMR spectroscopy could provide spectacular sensitivity/scan time advantages over ^{31}P for certain metabolic studies and clinical applications.

Key difficulties encountered with the implementation of *in vivo* ^{1}H metabolic spectroscopy are the suppression of H_2O and lipid —CH_2— resonances (21–23) and the method of spatial localization. The H_2O resonance is of order 10,000-fold more intense than the metabolites and normally swamps the spectrum. Solvent-suppression techniques that rely on avoiding excitation of the H_2O resonance (24) are unsuitable for localized spectroscopy schemes involving spatially selective excitation rf pulses because these excite the entire spectrum (20, 25). Thus, the best approach is to either selectively saturate the H_2O resonance or otherwise ensure that the net H_2O magnetization is nulled or directed parallel to the main field during data acquisition. The latter method has recently been used to separately image H_2O and lipid components in the head and limbs (20, 26). Suppression of the lipid —CH_2— signal is more difficult because its chemical shift essentially overlaps that of the lactate resonance (21–23). Fortunately, the NMR-detectable lipid concentration in brain and homogeneous muscle tissue is minute compared to that of adipose tissue (17, 18, 20–23, 25). The problem therefore shifts to that of providing sufficiently sharp spatial localization that surface adipose and other infiltrating tissue high in lipid content are effectively excluded from spectra.

We have combined spatially selective excitation (25) and H_2O suppression by chemical-selective irradiation NMR pulse sequences (20, 26) with surface coil detection (17, 18, 27) to observe ^{1}H metabolite-level spectra from the human brain. Spectra are acquired at 1.5 T in averaging periods of 2 s consistent with the expected sensitivity advantage of the ^{1}H nucleus. Spectroscopy sequences are immediately followed by conventional planar imaging with the same NMR coils (28, 29) to precisely determine the location and size of the spectroscopy volume element (voxel). Studies of the human arm and the head of a dog are also presented.

METHODS

In vivo experiments were performed on a 1.5-T, 1-m-bore Oxford Instruments superconducting magnet and a broadband quadrature phase-sensitive detection spectroscopy research system operating at 62.2 MHz with a spectrometer noise figure of around 0.8 dB (decibel) (17, 18). Resonance was excited with a 25-cm (diameter) saddle-shaped head-sized NMR coil with distributed capacitance and detected with either a 3-cm (diameter) or a 6.5-cm (diameter) surface coil. The transmitter and receiver rf fields were orthogonal and crossed diodes placed in series with the head coil and in parallel with the 6.5-cm coil to minimize mutual interactions. Crossed diodes were unnecessary in the smaller coil. In a homogeneous sample excited by a uniform rf field, the surface coil sensitivity profile of both coils is such that 50% of the total integrated NMR signal derived from a plane lying 5 cm deep and parallel to the coil falls within a 6.5-cm (radius) disk, as computed from the formula for the field component of a circular loop lying perpendicular to the main field (30).

The publication costs of this article were defrayed in part by page charge payment. This article must therefore be hereby marked "*advertisement*" in accordance with 18 U.S.C. §1734 solely to indicate this fact.

Abbreviations: *P*Cr, phosphocreatine; Cr, creatine; *P*Cho, phosphocholine; *N*-AcAsp, *N*-acetylaspartate.

The loaded signal-to-noise ratio (ψ) of a pure H_2O sample detected by the 6.5-cm (diameter) coil at a 5-cm depth (on axis) was measured at 38,000 $Hz^{1/2}$/ml by using the projection technique (31). Assuming a partial saturation factor of 0.71 ($T_1 \approx 0.8$ s), $T_2 \approx 0.1$ s, and two averages yield $\psi(H_2O) = 0.71 \times 38{,}000 \times 0.1^{1/2} = 8500$ per ml (31). A metabolite present at 10 mM concentrations (e.g., *N*-AcAsp) with comparable relaxation times is then detectable in the ^1H NMR spectrum with ψ (10 mM) $\approx$ 1.5 per ml, or ψ (10 mM) $\approx$ 50 from the 13-cm (diameter) sensitive disk, assuming a 5-mm slice thickness and an additional halving of ψ due to fading of the sensitivity profile off axis. The corresponding estimate for the 3-cm coil is ψ (10 mM) $\approx$ 25 in a spectrum averaging two acquisitions.

Four solvent-suppressed localized hydrogen spectroscopy NMR pulse sequences were investigated, as depicted in Fig. 1. Sequences shown in Fig. 1 *a* and *b* employ a 100-ms duration, sinc function amplitude-modulated $\pi/2$ rf pulse of 0.7 ppm measured linewidth in the frequency domain centered on the H_2O resonance, for subsequent H_2O suppression. The chemical-selective pulse is followed by a conventional $\pi/2$ sinc function modulated slice-selective pulse applied in the presence of a magnetic field gradient (G_y) directed perpendicular to the NMR surface coil used for detection (25). This excites all of the nuclei in a selected plane parallel to the surface coil and affects a π net nutation to the H_2O magnetization, thereby rendering it in principle unobservable (20). There is no need to change the rf of the slice-selective pulse because its bandwidth is much greater than the range of chemical shifts present in the sample. A 5-mm-thick slice was used throughout. The amplitude of the H_2O-selective pulse is adjusted for maximal annihilation of the H_2O resonance during data acquisition (20). The remaining NMR signal is then either detected immediately following the slice-selective pulse (sequence in Fig. 1*a*) or refocused to a spin echo by using a subsequent (nonselective) π pulse at time τ following the $\pi/2$ pulse (sequence in Fig. 1*b*). The latter sequence provides additional attenuation of any inherently broad H_2O resonance component with short NMR spin–spin relaxation time (T_2).

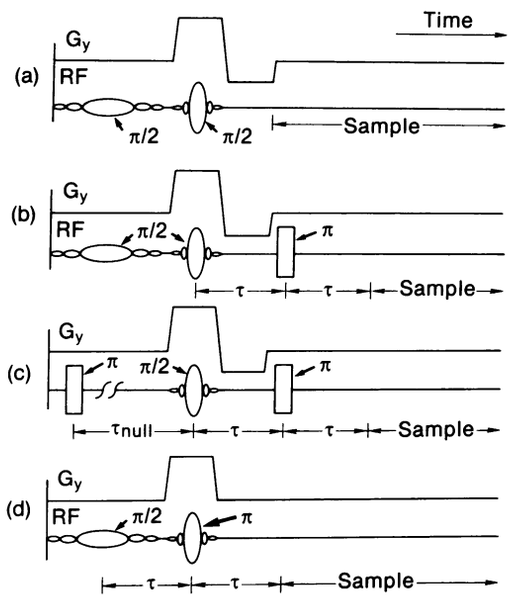

FIG. 1. (*a–d*) Timing diagram for four methods of performing solvent-suppressed chemical-shift spectroscopy. G_y is the amplitude of a linear magnetic field gradient directed coaxial to the surface detection coil ($G_y = \partial B_o/\partial_y$, where B_o is the main magnetic field); rf is the envelope of the rf NMR pulses; π and $\pi/2$ denote the effective nutation angles (amplitude) of the rf pulses; τ is the period between $\pi/2$ and π pulses in a spin-echo NMR sequence; τ_{null} is the period between π and $\pi/2$ pulses in an inversion recovery T_1-null sequence; and sample denotes the data acquisition period. Selective pulses are depicted as sinc-function modulated envelopes: they are chemical-shift selective when applied in the absence of the G_y gradient and spatially selective in the presence of the gradient. A negative G_y lobe is not required in *d* if the π pulse is symmetrically located with respect to the positive G_y lobe. Slice-selective pulses are phase alternated in a subsequent application of each sequence and the NMR data are subtracted to eliminate spurious signals from the other pulses.

Discrimination on the basis of relaxation times is extended in the sequence shown in Fig. 1*c*, wherein the chemical-selective pulse is abandoned to be replaced by an initial π inversion pulse applied at time τ_{null} preceding the slice-selective $\pi/2$ pulse. τ_{null} is adjusted to eliminate the H_2O resonance at $\tau_{null} \approx 0.69\ T_1$ (H_2O), where T_1 is the spin-lattice relaxation time. Inversion pulses are used in a similar fashion for solvent suppression in conventional NMR spectroscopy (32). The sequence shown in Fig. 1*d* is a reduction of that in Fig. 1*b*, in which the initial $\pi/2$ excitation pulse is a chemical-selective pulse tailored to select only the metabolically useful portion of the ^1H spectrum, excluding the H_2O resonance. Slice selection is subsequently performed by the π refocusing pulse applied in the presence of the gradient. In all cases, data were averaged from two applications of the sequences repeated at 1-s periods with the phase of the $\pi/2$ excitation pulse alternated to remove unwanted spurious signals generated by the other rf pulses (33).

The magnetic field homogeneity was shimmed for the narrowest linewidth of the H_2O resonance with resistive shim gradient coils during application of the desired solvent-suppressed localized hydrogen spectroscopy sequence with solvent suppression turned off (20). Typically, 0.1- to 0.2-ppm linewidths were achieved on the head with all surface coils. This procedure enabled compensation for gradients occurring during data acquisition due to eddy currents induced in the magnet cryostat or structural metal by the slice-selection gradient (20, 25). However, shimming precludes use of any external or internal spectrometer reference standards for assigning absolute chemical-shift values. Instead, the chemical shifts of H_2O and lactate (—CH_3) at 37°C were measured with a Varian XL300 300-MHz high-resolution NMR spectrometer at 4.67 ppm and 1.32 ppm (doublet), respectively, relative to sodium trimethylsilylpropionate, and the observed chemical shift of a prominent brain resonance assigned to *N*-AcAsp at 2.03 ppm (21, 23) served as spectral reference markers. Absence of substantial lipid —CH_2— resonances (0.9–1.7 ppm) in the ^1H spectrum is indicative of satisfactory spectroscopy voxel localization in (normal) muscle or brain tissue (20, 25).

Spectroscopy experiments were repeated on five conscious adult male volunteers and on a dog anesthetized with sodium pentobarbital (25 mg/kg) to serve as a control for studies involving pathology models. Raw spectroscopy data were multiplied by a 100-ms time constant exponential filter, complex Fourier transformed, baseline flattened by using a convolution difference method (27), and corrected for zeroth and first-order phase drift. Conventional *spin warp* spin-echo planar imaging (18, 28, 29) was then performed with the identical coil set and slice-selection characteristics as used for spectroscopy, without moving or disturbing the subject. Transition from spectroscopy to imaging operation modes requires only readjustment of the spectrometer data acquisition filter bandwidths and recall of a new imaging pulse sequence program from the operating computer. Image arrays consist of 256 × 256 0.9 mm × 0.9 mm resolution picture points recorded in 102 s (0.2-s sequence repetition period) or 512 s (1.0-s sequence repetition period).

RESULTS

Solvent suppression of brain H_2O in a selected plane 4 cm deep in the human head with sequences of Fig. 1 *b* and *c* is demonstrated in Fig. 2 *a* and *c*, respectively. The H_2O signal in the spectrum of Fig. 2*b* is attenuated 33-fold in integrated area compared to the spectrum of Fig. 2*a* and shows a notched profile characteristic of the chemical-selective irradiation pulse. In the spectrum shown in Fig. 2*c*, where H_2O is suppressed by adjustment of τ_{null}, only a reduction in H_2O amplitude by a factor of about 20 ensued. This proved inadequate to prevent obliteration of *P*Cho/*P*Cr/Cr resonances in the region 3.0–3.3 ppm. The sequence shown in Fig. 1*a* produced comparable results to that of Fig. 1*b*, but an excessive broad baseline component in brain spectra rendered phasing difficult. Recording spin-echo data with the sequence of Fig. 1*b* 40–160 ms (τ = 20–80 ms) after slice selection provided adequate suppression of this short T_2 component in brain studies. The sequence shown in Fig. 1*d* produced essentially equivalent results to that of Fig. 1*b*.

Initially, attempts were made to observe lactate development in muscle during exercise because of the success of ^{31}P NMR in muscle studies (13–15). The sequence in Fig. 1*a* with the 6.5-cm coil and two averages was employed. Dramatic changes between resting and exercised arm ^1H spectra occur in the peak at 1.3 ppm in Fig. 3 *a* and *b*, but the corresponding images (Fig. 3 *c* and *d*) indicate that the source of the variation is intrusion of bone marrow lipid into the selected slice as the internal anatomy distorts during muscular contraction. Some metabolite level resonances are discernible in the baseline, but the 0.6- to 2.0-ppm region of the spectra is swamped by lipid.

Fig. 4*a* is a normal human brain spectrum recorded in 2 s with the sequence of Fig. 1*b* (τ = 20 ms) and 3-cm coil. The selected plane was saggital and located 5 cm deep from the surface of the head. A spectrum from the dog head acquired with the 3-cm coil, 2-s averaging time, 5-cm-deep selected saggital plane, and the sequence of Fig. 1*b* (τ = 80 ms) is shown in Fig. 4*b*. The signal-to-noise ratio of the *N*-AcAsp resonance is consistent with the H_2O measurement/calculations. Images in Fig. 4 *c* and *d* illustrate the sensitivity profiles in the sample across the same saggital slices corresponding to the selected volumes represented by the spectra in Fig. 4 *a* and *b*, respectively. The images verify that lipid signal contributions to the selected plane from scalp tissue are minimal. However, it is evident from the image in Fig. 4*d* that only about half of the ^1H NMR signal in the dog spectrum derives from the brain. The image in Fig. 4*e* shows the effect in the human head of increasing the surface coil size to 6.5 cm: the relative lipid signal amplitude was roughly tripled and the signal-to-noise ratio was doubled. The image in Fig. 4*f* is a transaxial scan corresponding to Fig. 4*e* showing the slice location in the human head. By comparison, a ^{31}P spectrum recorded from a similar-sized localized volume in the brain with a 1-s repetition period and 6.5-cm (diameter) surface coil required a 20-min averaging period (25) to achieve a comparable signal-to-noise ratio.

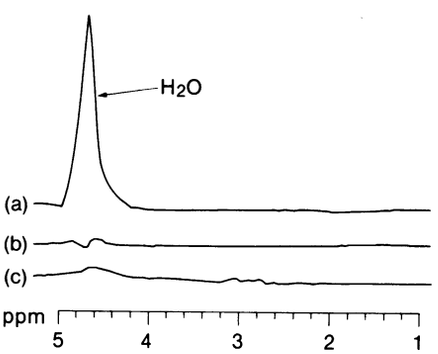

FIG. 2. Depth-resolved ^1H spectra recorded from a 4-cm-deep selected slice in the brain with a 3-cm (diameter) surface coil located above the temple. Sequences of Fig. 1 *b* and *c* were used to obtain the spectra in *b* and *c*, respectively. The spectrum in *a* was acquired with the solvent-suppression portion of the sequences turned off. Each spectrum is an average of two signals recorded at 1-s periods.

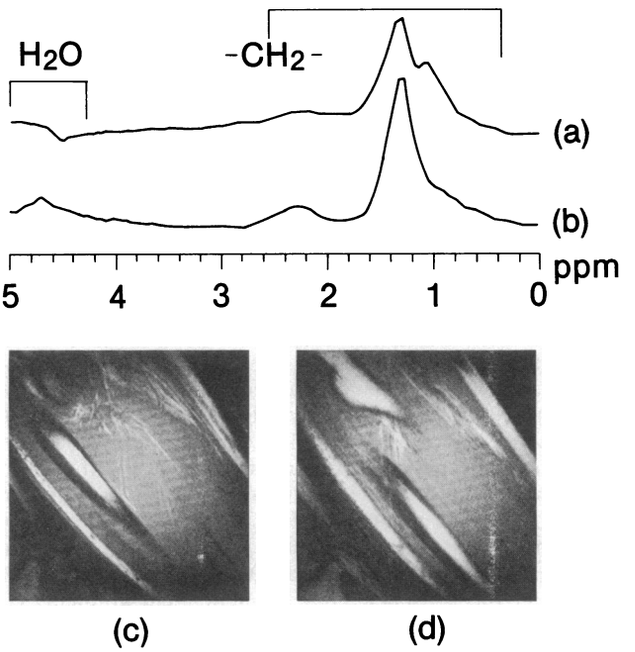

FIG. 3. ^1H spectra recorded from the forearm before (*a*) and during (*b*) exercise with the sequence of Fig. 1*a*, the 6.5-cm (diameter) surface coil, and a 2-s averaging time. Images in *c* and *d* show the selected volumes corresponding to the spectra in *a* and *b*, respectively. Images were recorded in 102 s with a 0.2-s repetition period. Adipose, marrow, and tissue high in mobile lipid appear bright (—CH_2— = lipid resonances).

DISCUSSION

Clearly, lipid contamination of spectra is problematic, particularly in muscle spectra. Devising localization schemes that spatially discriminate against lipid signals lying outside the selected volume with attenuation factors of more than 1000-fold is a nontrivial feat. However, since shimming for optimal magnetic field homogeneity within the selected volume inevitably degrades the homogeneity outside the volume, external lipid resonances are broadened and even shifted relative to the spectral markers. In the head, such broad components are largely eliminated by the baseline flattening operation. This effect is analogous to the "topical magnetic resonance" localization technique for spectroscopy (34) and is likely responsible for differences between lipid regions of the human head and dog spectra (compare spatial distributions of adipose/lipid tissues in Fig. 4 *a* and *b*) as well as the improved lipid suppression achieved with the 3-cm coil compared to the 6-cm coil. The calculations of the rf coil sensitivity profiles do not take this into account.

Techniques for eliminating lipid signals derived from within the selected volume would be necessary for investigations of lactate metabolism in pathologies such as muscular dystrophy and liver cirrhosis. One method for isolating the lactate (—CH_3) resonance contribution is to record spectra with and without selective NMR decoupling of other lactate nuclei and calculate a difference spectrum (35). Another possibility is to add an inversion pulse prior to the sequence

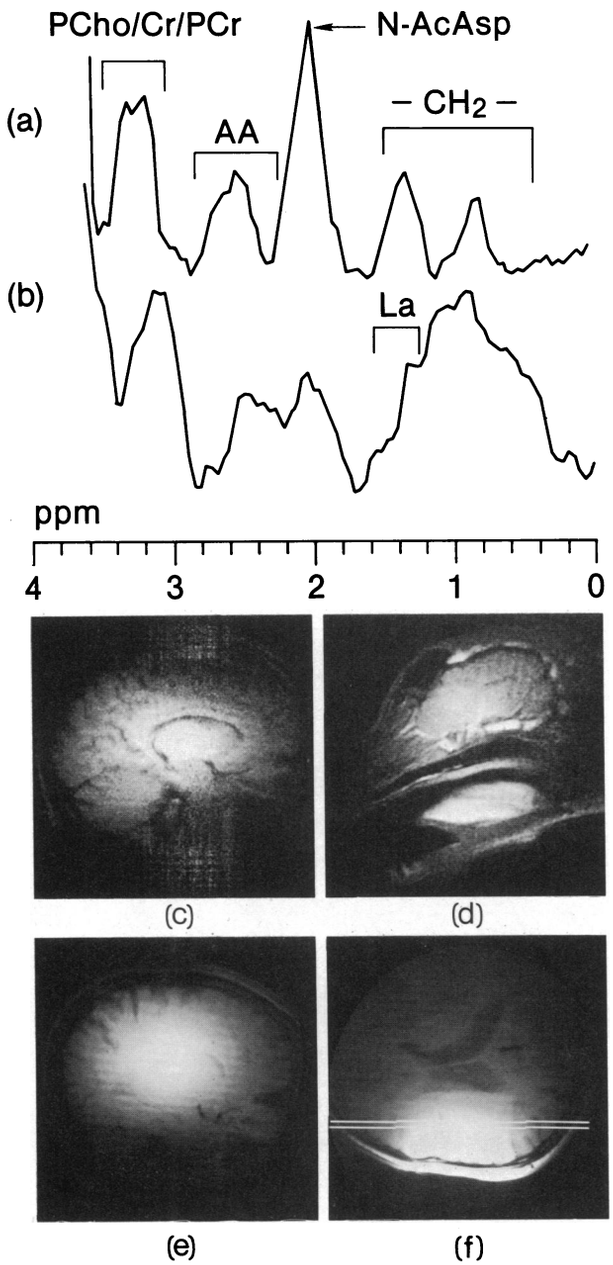

FIG. 4. (*a* and *b*) Typical normal localized ^1H spectrum from a human brain and a dog head, respectively, recorded *in vivo* with the sequence of Fig. 1*b* selecting 5-mm-thick saggital slices at a depth of 5 cm in 2 s using the 3-cm (diameter) coil. Images in *c* and *d* show the sample distribution across the selected slices in the human and dog experiments corresponding to the voxels of the respective localized spectra, as recorded with the same 3-cm coil. Images in *e* and *f* illustrate the voxel selected by the 6.5-cm (diameter) coil placed on the human head: *e* is a saggital scan similar to *c*, and *f* shows the corresponding transaxial scan with the location and thickness of the slice indicated. Images were obtained in 512 s with a 1.0-s repetition period. [*P*Cho/*P*Cr/Cr = *P*Cho and total Cr pool; AA = amino acids including aspartyl group, glutamate, and glutamine (21, 23); —CH_2— = lipid resonance; La denotes the potential location of the lactate —CH_3 resonance.]

of Fig. 1*b* and adjust τ_{null} to minimize the lipid at $\tau_{null} \approx 0.69$ T_1 (lipid) in the H_2O-suppressed spectrum.

The ability to acquire metabolite-level localized ^1H NMR spectra on such a rapid time scale compared to ^{31}P raises the possibility that the lactate resonance might be usefully imaged. However, this would be difficult using chemical-selective pulses for H_2O suppression due to the problem of obtaining sufficiently high magnetic field homogeneity across the whole head (20). The use of conventional surface coil NMR imaging with depth-localized spectroscopy is nevertheless a valuable adjunct for determining the precise nature of the selected volume under investigation.

We thank C. Daniels for assistance and provision of animals, E. A. Williams for provision of the 300-MHz spectra, and H. R. Hart, W. M. Leue, O. M. Mueller, R. W. Redington, J. F. Schenck, L. S. Smith, and D. Vatis for valuable contributions to our NMR imaging/spectroscopy system.

1. Shoubridge, E. A., Briggs, R. W. & Radda, G. K. (1982) *FEBS Lett.* **140,** 288–292.
2. Bottomley, P. A., Kogure, K., Namon, R. & Alonso, O. F. (1982) *Magn. Reson. Imaging* **1,** 81–85.
3. Thulborn, K. R., du Boulay, G. H., Duchen, L. W. & Radda, G. (1982) *J. Cereb. Blood Flow Metab.* **2,** 299–306.
4. Prichard, J. W., Alger, J. R., Behar, K. L., Petroff, O. A. C. & Shulman, R. G. (1983) *Proc. Natl. Acad. Sci. USA* **80,** 2748–2751.
5. Decorps, M., Lebas, J. F., Leviel, J. L., Confort, S., Remy, C. & Benabid, A. L. (1984) *FEBS Lett.* **168,** 1–6.
6. Nunnally, R. L. & Hollis, D. P. (1979) *Biochemistry* **18,** 3642–3646.
7. Grove, T. H., Ackerman, J. J. H., Radda, G. K. & Bore, P. J. (1980) *Proc. Natl. Acad. Sci. USA* **77,** 299–302.
8. Koretsky, A. P., Wang, S., Murphy-Boesch, J., Klein, M. P., James, T. L. & Weiner, M. W. (1983) *Proc. Natl. Acad. Sci. USA* **80,** 7491–7495.
9. Ng, T. C., Evanochko, W. T., Hiramoto, R. N., Ghanta, V. K., Lilly, M. B., Lawson, A. J., Corbett, T. H., Durant, J. R. & Glickson, J. D. (1982) *J. Magn. Reson.* **49,** 271–286.
10. Evanochko, W. T., Ng, T. C., Lilly, M. B., Lawson, A. J., Corbett, T. H., Durant, J. R. & Glickson, J. D. (1983) *Proc. Natl. Acad. Sci. USA* **80,** 334–338.
11. Nunnally, R. L. & Bottomley, P. A. (1981) *Science* **211,** 177–180.
12. Mathews, P. M., Williams, S. R., Seymour, A. M., Schwartz, A., Dube, G., Gadian, D. G. & Radda, G. K. (1982) *Biochim. Biophys. Acta* **720,** 163–171.
13. Ross, B. D., Radda, G. K., Gadian, D. G., Rocker, G., Esiri, M. & Falconer-Smith, J. (1981) *N. Engl. J. Med.* **304,** 1338–1342.
14. Radda, G. K., Bore, P. J., Gadian, D. G., Ross, B. D., Styles, P., Taylor, D. G. & Morgan-Hughes, J. (1982) *Nature (London)* **295,** 608–609.
15. Edwards, R. H. T., Dawson, M. J., Wilkie, D. R., Gordon, R. E. & Shaw, D. (1982) *Lancet* **i,** 725–731.
16. Cady, E. B., de L. Costello, A. M., Dawson, M. J., Delpy, D. T., Hope, P. L., Reynolds, E. O. R., Tofts, P. S. & Wilkie, D. R. (1983) *Lancet* **i,** 1059–1062.
17. Bottomley, P. A., Hart, H. R., Edelstein, W. A., Schenck, J. F., Smith, L. S., Leue, W. M., Mueller, O. M. & Redington, R. W. (1983) *Lancet* **ii,** 273–274.
18. Bottomley, P. A., Hart, H. R., Edelstein, W. A., Schenck, J. F., Smith, L. S., Leue, W. M., Mueller, O. M. & Redington, R. W. (1984) *Radiology* **150,** 441–446.
19. Becker, E. D. (1969) *High Resolution NMR* (Academic, New York), pp. 241–251.
20. Bottomley, P. A., Foster, T. H. & Leue, W. M. (1984) *Proc. Natl. Acad. Sci. USA* **81,** 6856–6860.
21. Behar, K. L., den Hollander, J. A., Stromski, M. E., Ogino, T., Shulman, R. G., Petroff, O. A. C. & Prichard, J. W. (1983) *Proc. Natl. Acad. Sci. USA* **80,** 4945–4948.
22. Ugurbil, K., Petein, M., Maidan, R., Michurski, S., Cohn, J. N. & From, A. H. (1984) *FEBS Lett.* **167,** 73–78.
23. Behar, K. L., Rothman, D. L., Shulman, R. G., Petroff, O. A. C. & Prichard, J. W. (1984) *Proc. Natl. Acad. Sci. USA* **81,** 2517–2519.
24. Hore, P. J. (1983) *J. Magn. Reson.* **55,** 283–300.
25. Bottomley, P. A., Foster, T. H. & Darrow, R. D. (1984) *J. Magn. Reson.* **59,** 338–342.
26. Bottomley, P. A., Foster, T. H. & Leue, W. M. (1984) *Lancet* **i,** 1120.
27. Ackerman, J. J. H., Grove, T. H., Wong, G. G., Gadian, D. G. & Radda, G. K. (1980) *Nature (London)* **283,** 167–170.

28. Bottomley, P. A., Edelstein, W. A., Hart, H. R., Schenck, J. F. & Smith, L. S. (1984) *Magn. Reson. Med.* **1,** 410–413.
29. Edelstein, W. A., Schenck, J. F., Hart, H. R., Hardy, C. J., Foster, T. H. & Bottomley, P. A. (1985) *J. Am. Med. Assoc.* **253,** 828.
30. Smythe, W. R. (1939) *Static and Dynamic Electricity* (McGraw-Hill, New York), pp. 266–268.
31. Edelstein, W. A., Bottomley, P. A. & Pfeifer, L. M. (1984) *Med. Phys.* **11,** 180–185.
32. Martin, J. L., Martin, G. J. & Delpuech, J. J. (1980) *Practical NMR Spectroscopy* (Heyden, London), pp. 275–280.
33. Edelstein, W. A. & Bottomley, P. A. (1984) U.S. patent 4,443,760.
34. Gordon, R. E., Hanley, P. E., Shaw, D., Gadian, D. G., Radda, G. K., Styles, P., Bore, P. J. & Chan, L. (1980) *Nature (London)* **287,** 736–738.
35. Rothman, D. L., Arias-Mendoza, F., Shulman, G. I. & Shulman, R. G. (1984) *J. Magn. Reson.* **60,** 430–436.